3b2 Version Number : 7.00a/W (Sep 25 2000)
File path : p:/Santype/Journals/Taylor&Francis/Nht/44(2)/44(2)-8901/NHT44(2)-8901.3d
Date and Time : 19/5/03 and 13:31

Numerical Heat Transfer, Part A, 44: 1–29, 2003

ISSN: 1040-7782 print/1521-0634 online
DOI: 10.1080/10407780390219469

Taylor & Francis
Taylor & Francis Group

THE METHOD OF CONSTRUCTING DYNAMICALLY ADAPTING GRIDS FOR PROBLEMS OF UNSTABLE LAMINAR COMBUSTION

V. I. Mazhukin
Institute of Mathematical Modeling, Russian Academy of Sciences, Miusskaya sq. 4A, 125047, Moscow, Russia

I. Smurov
Ecole Nationale d'Ingenieurs de Saint-Etienne, 58 rue Jean Parot, 42023, Saint-Etienne Cedex, France

A. V. Shapranov and M. M. Demin
Institute of Mathematical Modeling, Russian Academy of Sciences, Miusskaya sq. 4A, 125047, Moscow, Russia

The method of constructing dynamically adapting calculation grids for solving problems with unstable (relaxational or oscillatory) type of solution behavior is presented. Stable and pulsed modes of laminar combustion in a wide range of values of the Lewis number and activation energy are investigated using mathematical modeling. The efficiency of the method as to the operation speed and the number of nodes used is estimated. Mathematical modeling shows that application of dynamic adaptation makes it possible to reduce the number of grid nodes by 1–2.5 orders and increase the operation speed by 2–50 times.

INTRODUCTION

Calculation methods, such as the combustion theory in general, are far from being developed completely. Computational peculiarities of problems of laminar combustion are due to the presence of physical-chemical processes with greatly different typical times: a short time of a chemical reaction and a long time of thermal relaxation (the diffusion mechanism). Accordingly, a high rate of chemical transformation of the material and a slow propagation of thermal perturbations and diffusion mixing of the reacting mixture lead to formation of a narrow combustion zone with large gradients of the temperature T and the density ρ. The combustion front is usually initiated at one boundary and moves rapidly toward the opposite one. Numerical solution requires that a certain number of grid nodes should be present in the reaction zone. These two circumstances prevent discretizing the spatial

Received 7 August 2002; accepted 16 January 2003.
Address correspondence to I. Smurov, ENISE, 58 rue Jean Parot, 42023 Saint-Etienne Cedex, France. E-mail: smurov@enise.jr

NOMENCLATURE

A	pre-exponent	τ	computational time coordinate
A	thermal conductivity coefficient	Φ	thermal release function
C_p	heat capacity	ψ	transformation Jacobian
D	diffusion coefficient	$\Omega_{q,\tau}$	computational space
E	activation energy	$\Omega_{\tilde{x},\tilde{t}}$	physical space
H	mass heat of combustion		
K	temperature coefficient of the combustion velocity	**Subscripts**	
		0	signifies the initial magnitude of the variable
K	velocity coefficient		
L	domain spatial size	f	signifies value at free border
Le	Lewis number	i	signifies grid function in the ith (integer) node
Q	transformation function		
Q	computational space coordinate	$i+1/2$	signifies grid function in the $i+\frac{1}{2}$th (semi-integer) node
R	gas constant		
T	medium temperature	$0, L$	signifies left and right boundary values
T	physical time coordinate	1, 2	signifies that variable belongs to the first or second substance or reaction
X	physical space coordinate		
β	heat release coefficient		
$\delta_\rho; \delta_T$	thickness of diffusion and heat action zones	**Superscripts**	
		s	signifies iteration number
θ	dimensionless activation energy	j	signifies number of temporal layer
ρ	medium density	$\tilde{}$	signifies that variable is dimensional

variables with a large step using grids with fixed nodes. When the ratios of the size L of the region under investigation to the combustion zone typical thickness δ are large, the efficiency of computational algorithms using grids with fixed nodes becomes much lower because of a large number of nodes to be used. Thus a conventional grid with fixed nodes applied for solving a typical problem of unstable combustion contains 3,000–5,000 nodes.

Experience in numerical modeling [1–7] shows that application of adapting grids greatly enhances the efficiency of computational algorithms, which is manifested in considerably increased accuracy of solution with simultaneous reduction of the number of nodes. They are of particular service in solving unstable problems involving rapidly moving narrow zones with large derivatives of the solution. Such problems include the problem of laminar flame propagation, in which, as has been mentioned above, a high rate of chemical transformation of the reactant and a slow velocity of propagation of thermal perturbations in the mixture that has not yet participated in the reaction result in formation of a narrow combustion zone with large gradients of the temperature and the concentration.

The main objective of theoretical study of the combustion process is to determine a normal velocity and mode of the flame propagation. Depending on the relation of a number of the thermophysical parameters of the medium, the flame front is propagated in either the stable (steady) mode or the unstable (pulsed) mode. Stable modes are characterized by a constant front propagation velocity and a stable thermodiffusion structure of the flame. The appearance of thermodiffusion instability is accompanied by violation of the similarity between the temperature and density distributions, and the front velocity may attain a complicated pulsed character.

A number of theoretical studies [8–11] have been devoted to finding the conditions for thermal stability in combustion of gaseous media. However, numerical modeling of unstable and self-oscillatory modes of combustion are still a rather hard computational problem [8], which is manifested, in particular, in the necessity of using calculation grids with a very large number of nodes [11].

The dynamical adaptation method for solving unstable problems has been suggested in [12, 13], and was found to be highly efficient in solving problems with mobile boundaries and large gradients of solution. Application of this method makes it possible to solve problems with automatic isolation of strong discontinuities, such as phase boundaries (interfaces) in Stephan multifront problems [14, 15] and shock waves in gas dynamics [16]. In problems of the Burgers type, the application of dynamic adaptation [17] has improved considerably the quality of difference schemes at the expense of almost total elimination of the influence of their diffusion and dissipative properties. Ultimately, this allowed reducing the number of the nodes used by 2–3 orders as compared to grids with fixed nodes. However, the dynamical adaptation method, in which the transformation function is found from the quasi-stationarity principle, has never been applied to solving problems whose solutions are of oscillation type.

The aim of the present work is to extend the dynamical adaptation method to mathematical modeling of different stable, unstable, and self-oscillation modes of laminar flame. In this way it will be possible to determine the efficiency of the method as to its operation speed and the number of the nodes to be used.

MATHEMATICAL FORMULATION OF THE PROBLEM

We consider a model problem of flame front propagation in a homogeneous (as to temperature and density), motionless gaseous medium. It is assumed that the chemical reaction wave is propagated at a subsonic velocity, the combustion process is isobaric, and the transfer of heat and matter has a diffusion nature. The kinetic energy of the gas is negligible as compared to the heat content. The total enthalpy of the system is the sum of the thermal and chemical energies, which is constant under stationary conditions.

The Model of One-Stage Combustion

In the simplest case of one-stage combustion, the exothermic reaction thermal release function Φ depends linearly on the medium density ρ and exponentially (according to the Arrhenius law) on the temperature T:

$$\Phi(\tilde{T}, \tilde{\rho}_1) = h_1 \tilde{\rho}_1 k_1 e^{-E_1/R\tilde{T}} \tag{1}$$

where h is the mass heat of combustion, k is the velocity coefficient, E is the activation energy, and R is the gas constant.

In the adopted assumptions the laminar flame propagation problem in the simplest formulation is described by the system of two differential equations of the parabolic type: the equations for thermal conductivity and diffusion with constant coefficients of thermal conductivity a and diffusion D. In the physical space

$\Omega_{\tilde{x},\tilde{t}}$ with the variables $\tilde{t}$ and $\tilde{x}$ in a dimensional form, the mathematical model has the form:

$$\frac{\partial \tilde{\rho}_1}{\partial t} = D\frac{\partial^2 \tilde{\rho}_1}{\partial \tilde{x}^2} - \frac{\tilde{\Phi}_1(\tilde{T}, \rho_1)}{h_1} \tag{2}$$

$$C_p \rho_0 \frac{\partial \tilde{T}}{\partial \tilde{t}} = \lambda \frac{\partial^2 \tilde{T}}{\partial \tilde{x}^2} + \tilde{\Phi}_1(\tilde{T}, \rho_1) \tag{3}$$

$$0 = \tilde{x}_0 \le \tilde{x} \le \tilde{x}_L = L \qquad t \ge 0$$

where L is the length of the region under consideration.

In the problem of laminar (layer-by-layer) combustion, or combustion in the front, one of the most important factors affecting the flame front propagation mode is the ratio of the transfer coefficients: the diffusion coefficient D and the thermal conductivity coefficient a. Depending on their relation (the D-to-a ratio is referred to as the Lewis number, $\mathrm{Le} = D/a$), combustion has either a stationary character, $\mathrm{Le} = 1$, when the total enthalpy is constant in the flame, or a pulse character, $\mathrm{Le} \neq 1$, when the sum of the thermal and chemical energies is not constant. The farther the Lewis number deviates from unity, the greater is the destabilizing effect. The equality $\mathrm{Le} = 1$ corresponds formally to combustion of a condensed substance.

The Model of Two-Stage Combustion

In the majority of cases, chemical reactions in flames proceed by a multistage scheme. With a multistage mechanism of chemical transformation the flame front structure is much more complex than in the case of a one-stage reaction and is determined by interaction of different stages. The peculiarity of a mathematical description of flame in multistage reactions is that it is necessary to formulate and solve differential equations for concentrations of the components that are absent in the initial and final states of the combustible mixture. Formally, the simplest scheme of multistage combustion of the combustible mixture can be obtained by taking into account two chemical reactions characterized by two heat release functions $\tilde{\Phi}_1$ and $\tilde{\Phi}_2$ [8]:

$$\tilde{\Phi}_1(\tilde{T}, \tilde{\rho}_1) = h_1 \tilde{\rho}_1 k_1 \exp\left(-\frac{E_1}{R\tilde{T}}\right) \qquad \tilde{\Phi}_2(\tilde{T}, \tilde{\rho}_2) = h_2 \tilde{\rho}_2 k_2 \exp\left(-\frac{E_2}{R\tilde{T}}\right) \tag{4}$$

where the index 2 signifies that the values $h_2, \tilde{\rho}_2, k_2, E_2$ refer to the second chemical reaction.

The mathematical model of two-stage combustion with two chemical reactions has the form:

$$\frac{\partial \tilde{\rho}_1}{\partial \tilde{t}} = D_1 \frac{\partial^2 \tilde{\rho}_1}{\partial \tilde{x}^2} - \frac{\tilde{\Phi}_1(\tilde{T}, \tilde{\rho}_1)}{h_1} \tag{5}$$

$$\frac{\partial \tilde{\rho}_2}{\partial \tilde{t}} = D_2 \frac{\partial^2 \tilde{\rho}_2}{\partial \tilde{x}^2} - \frac{\tilde{\Phi}_2(\tilde{T}, \tilde{\rho}_2)}{h_2} + \frac{\tilde{\Phi}_1(\tilde{T}, \tilde{\rho}_1)}{h_1} \tag{6}$$

$$C_p \rho_0 \frac{\partial \tilde{T}}{\partial \tilde{t}} = \lambda \frac{\partial^2 \tilde{T}}{\partial \tilde{x}^2} + \tilde{\Phi}_1(\tilde{T}, \tilde{\rho}_1) + \tilde{\Phi}_2(\tilde{T}, \tilde{\rho}_2) \tag{7}$$

$$0 = \tilde{x}_0 \le \tilde{x} \le \tilde{x}_L = L \qquad t \ge 0$$

where $\tilde{\rho}_1$ and $\tilde{\rho}_2$ are the densities of the first and second substances; D_1, D_2, λ, C_p, and ρ_o are the coefficients of diffusion and thermal conductivity, the specific heat, and the initial density of the first substance; E_1, E_2, h_1, and h_2 are the activation energies of the reactions and the mass heats of combustion; L is the length of the region under consideration.

Initial and Boundary Conditions

In choosing the value of L it was taken into account that in a typical internal combustion engine a characteristic dimension of the combustion chamber is 5 cm. In subsequent calculations the value of L was, as a rule, not greater than 10 cm, though it is not the limitation of the method used.

A chemical reaction in a substance is generally initiated at one boundary with the help of an external energy source and then the reaction front is propagated toward the opposite boundary. It is assumed that the energy source is a hot wall placed at the origin, $\tilde{x} = 0$. Its temperature varies by the linear law from the initial temperature $\tilde{T}_0$ up to the so-called adiabatic temperature of combustion $\tilde{T}_a = \tilde{T}_0 + (h_1 + h_2)/C_p, \tilde{T}_0 \tilde{T} \tilde{T}_a$. The substance flow at the left boundary is taken to equal zero. These assumptions correspond to the following relations:

$$\tilde{x} = 0: \quad \tilde{T}(x_0, t) = \begin{cases} \tilde{T}_0 + ct, & t \le \frac{1}{c} \\ \tilde{T}_a, & t > \frac{1}{c} \end{cases} \qquad - D_1 \frac{\partial \tilde{\rho}_1(0, \tilde{t})}{\partial \tilde{x}} = -D_2 \frac{\partial \tilde{\rho}_2(0, \tilde{t})}{\partial \tilde{x}} = 0 \tag{8}$$

where c is a certain constant.

The opposite, right-hand end of the rod $\tilde{x} = \tilde{x}_L$ is taken to be isolated in thermal and diffusion respects:

$$\tilde{x} = \tilde{x}_L: \quad -\lambda \frac{\partial \tilde{T}(\tilde{x}_L, \tilde{t})}{\partial \tilde{x}} = 0 \qquad - D_1 \frac{\partial \tilde{\rho}_1(\tilde{x}_L, \tilde{t})}{\partial \tilde{x}} = -D_2 \frac{\partial \tilde{\rho}_2(\tilde{x}_L, \tilde{t})}{\partial \tilde{x}} = 0 \tag{9}$$

The initial value of temperature $\tilde{T}(0, \tilde{t})$ is chosen from the condition that the thermal release velocity function $\tilde{\Phi}(\tilde{T}, \tilde{\rho}_1, \tilde{\rho}_2)$ at a given temperature $\tilde{T}_0$ is equal to zero. The initial density $\tilde{\rho}_1(0, \tilde{t})$ is taken to equal the density of an unperturbed gas ρ_0:

$$\tilde{t} = 0: \qquad \tilde{T}(0, \tilde{t}) = \tilde{T}_0 \qquad \tilde{\rho}_1(0, \tilde{t}) = \rho_0 \tag{10}$$

Dimensionless Variables

The obtained differential models (3)–(10) are conveniently analyzed and solved if they are written in a dimensionless form. To make the transition, the following relations are used:

$$a = \frac{\lambda}{C_p \rho_o} \qquad \mathrm{Le}_1 = \frac{D_1}{a} \qquad \mathrm{Le}_2 = \frac{D_2}{a} \qquad A_1 = \frac{k_1 L^2}{a} \qquad A_2 = \frac{k_2 L^2}{a}$$

$$T = \frac{\tilde{T} C_p}{h_1 + h_2}$$

$$\beta_1 = \frac{h_1}{h_1 + h_2} \qquad \beta_2 = \frac{h_2}{h_1 + h_2} \qquad \beta_1 + \beta_2 = 1 \qquad \rho_1 = \frac{\tilde{\rho}_1}{\rho_o} \qquad \rho_2 = \frac{\tilde{\rho}_2}{\rho_o}$$

$$x = \frac{\tilde{x}}{L} \qquad t = \frac{a\tilde{t}}{L^2}$$

$$\theta_1 = \frac{E_1 C_p}{R(h_1 + h_2)} \qquad \theta_2 = \frac{E_2 C_p}{R(h_1 + h_2)} \qquad \Phi_k(T, \rho_k) = \beta_k \rho_k A_k \exp\left(-\frac{\theta_k}{T}\right)$$

$$k = 1, 2$$

The systems of equations (2)–(3) and (5)–(7) in dimensionless variables are

$$\frac{\partial \rho_1}{\partial t} = \mathrm{Le} \frac{\partial^2 \rho_1}{\partial x^2} - \rho_1 A_1 \exp\left(-\frac{\theta_1}{\mathrm{T}}\right) = -\mathrm{Le} \frac{\partial J_1}{\partial x} - \Phi_1(T, \rho_1) \tag{11}$$

$$\frac{\partial T}{\partial t} = \frac{\partial^2 T}{\partial x^2} + \rho_1 A_1 \exp\left(-\frac{\theta_1}{\mathrm{T}}\right) = -\frac{\partial W}{\partial x} + \Phi_1(T, \rho_1) \tag{12}$$

$$0 = x_0 \le x \le x_L = 1 \qquad t \ge 0$$

and

$$\frac{\partial \rho_1}{\partial t} = \mathrm{Le} \frac{\partial^2 \rho_1}{\partial x^2} - \rho_1 A_1 \exp\left(-\frac{\theta_1}{\mathrm{T}}\right) = -\mathrm{Le} \frac{\partial J_1}{\partial x} - \beta_1^{-1} \Phi_1(T, \rho_1) \tag{13}$$

$$\begin{aligned} \frac{\partial \rho_2}{\partial t} &= \mathrm{Le} \frac{\partial^2 \rho_2}{\partial x^2} - \rho_2 A_2 \exp\left(-\frac{\theta_2}{\mathrm{T}}\right) + \rho_1 A_1 \exp\left(-\frac{\theta_1}{\mathrm{T}}\right) \\ &= -\mathrm{Le} \frac{\partial J_2}{\partial x} - \beta_2^{-1} \Phi_2(T, \rho_2) + \beta_1^{-1} \Phi_1(T, \rho_1) \end{aligned} \tag{14}$$

$$\begin{aligned} \frac{\partial T}{\partial t} &= \frac{\partial^2 T}{\partial x^2} + \beta_1 \rho_1 A_1 \exp\left(-\frac{\theta_1}{\mathrm{T}}\right) + \beta_2 \rho_2 A_2 \exp\left(-\frac{\theta_2}{\mathrm{T}}\right) \\ &= -\frac{\partial W}{\partial x} + \Phi_1(T, \rho_1) + \Phi_2(T, \rho_2) \end{aligned} \tag{15}$$

$$J_1 = -\frac{\partial \rho_1}{\partial x} \qquad J_2 = -\frac{\partial \rho_2}{\partial x} \qquad W = -\frac{\partial T}{\partial x} \qquad 0 = x_0 \le x \le x_L = 1 \qquad t \ge 0$$

System (13)–(15) is written in the assumption of the equality of the diffusion coefficients of all the components of the combustible mixture $D = D_1 = D_2$. Accordingly, the Lewis number is $\mathrm{Le} = \mathrm{Le}_1 = \mathrm{Le}_2$.

The boundary and initial conditions in dimensionless variables assume the form:

$$x = 0: \qquad T(x_0, t) = \begin{cases} T_0 + ct, & t \le \frac{1}{c} \\ T_a, & t > \frac{1}{c} \end{cases} \qquad J_1(x_0, t) = J_2(x_0, t) = 0 \quad (16)$$

$$x = 1: \qquad J_1(x_L, t) = J_2(x_L, t) = W(x_L, t) = 0 \quad (17)$$

$$t = 0: \qquad T(x, 0) = T_0 \qquad \rho(x, 0) = \rho_0 \quad (18)$$

In the equations obtained, the density ρ_1 ranges from unity to zero. In the absence of an external heat supply the value of dimensionless temperature T lies in the interval $T_0 \le T \le T_a$, where $T_a = 1 + T_0$. In the present study the chosen values of the parameters correspond to combustion of hydrocarbon fuel in air, which is characterized by a sixfold increase of temperature [18]. Therefore the vale of $T = 0.2$ is taken as an initial condition, which gives $T_a/T_0 = 6$.

THE METHOD OF DYNAMIC ADAPTATION

To solve numerically the mathematical models (11)–(12) and (13)–(14) under the conditions (16)–(18), we apply the method of dynamic adaptation. The calculation grid is constructed on the basis of transition to an arbitrary nonstationary system of coordinates with the variables (q, τ), the system of coordinates belonging to a computational space $\Omega_{q,\tau}$. The transformation of the coordinates is made with the help of the sought solution. The inverse transformation equation that is a differential equation in partial derivatives is composed in such a way that the node movement velocity depends on the dynamics of solving the equations describing the physical processes involved.

Nonstationary Arbitrary System of Coordinates

The transition from the physical space $\Omega_{x,t}$ to the computational space $\Omega_{q,\tau}$ is made by substitution of a general kind, $x = \xi(q, \tau), t = \tau$, the substitution having an inverse transformation $q = \varphi(q, \tau), \tau = t$. The Jacobian of such transformation is the function $\psi = \partial x/\partial q$. The partial derivatives of the dependent variables are expressed in the following way:

$$\frac{\partial}{\partial t} = \frac{\partial}{\partial \tau} + \frac{\partial q}{\partial t}\frac{\partial}{\partial q} = \frac{\partial}{\partial \tau} - \frac{\partial x}{\partial \tau}\frac{1}{\psi}\frac{\partial}{\partial q} = \frac{\partial}{\partial \tau} + \frac{Q}{\psi}\frac{\partial}{\partial q}$$

$$\frac{\partial}{\partial x} = \frac{\partial q}{\partial x}\frac{\partial}{\partial q} = \frac{1}{\psi}\frac{\partial}{\partial q} \qquad \frac{\partial^2}{\partial x^2} = \frac{\partial q}{\partial x}\frac{\partial}{\partial q}\frac{\partial q}{\partial x}\frac{\partial}{\partial q} = \frac{1}{\psi}\frac{\partial}{\partial q}\frac{1}{\psi}\frac{\partial}{\partial q}$$

where $\partial x/\partial\tau = -Q$ is the velocity of the nonstationary coordinate system. In the new variables (q, τ) the systems of equations (11), (12), and (13)–(15) is written in the form:

$$\frac{\partial \rho_1}{\partial \tau} = -\mathrm{Le}\frac{1}{\psi}\frac{\partial J_1}{\partial q} - Q_1 J_1 - \Phi_1(T, \rho_1) \tag{19}$$

$$\frac{\partial T}{\partial \tau} = -\frac{1}{\psi}\frac{\partial W}{\partial q} - Q_1 W + \Phi_1(T, \rho_1) \tag{20}$$

$$\frac{\partial \psi}{\partial \tau} = -\frac{\partial Q_1}{\partial q} \qquad \frac{\partial x}{\partial q} = \psi \tag{21}$$

$$\frac{\partial \rho_1}{\partial \tau} = -\mathrm{Le}\frac{1}{\psi}\frac{\partial J_1}{\partial q} - Q_2 J_1 - \beta_1^{-1}\Phi_1(T, \rho_1) \tag{22}$$

$$\frac{\partial \rho_2}{\partial \tau} = -\mathrm{Le}\frac{1}{\psi}\frac{\partial J_2}{\partial q} - Q_2 J_2 - \beta_2^{-1}\Phi_2(T, \rho_2) + \beta_1^{-1}\Phi_1(T, \rho_1) \tag{23}$$

$$\frac{\partial T}{\partial \tau} = -\frac{1}{\psi}\frac{\partial W}{\partial q} - Q_2 W + \Phi_1(T, \rho_1) + \Phi_2(T, \rho_2) \tag{24}$$

$$\frac{\partial \psi}{\partial \tau} = -\frac{\partial Q_2}{\partial q} \qquad 0 = q_0 < q < q_L = 1 \qquad \tau \geq 0 \tag{25}$$

$$J_1 = -\frac{1}{\psi}\frac{\partial \rho_1}{\partial q} \qquad J_2 = -\frac{1}{\psi}\frac{\partial \rho_2}{\partial q} \qquad W = -\frac{1}{\psi}\frac{\partial T}{\partial q}$$

As a result of transition to the arbitrary nonstationary system of coordinates, the initial systems of differential equations are supplemented by the inverse transformation equations (21) and (25). After determining the particular form of the functions Q_1 and Q_2, these equations are used to construct the adapting grids. Their difference analog describes the grid node dynamics, and the functions Q_1 and Q_2 control the movement of the grid nodes matching the sought solution dynamics. Matching is achieved by the functional dependence of the functions Q_1 and Q_2 upon the sought solution, i.e., upon the functions ρ_1, ρ_2, T. A correct choice of the transformation function Q, provided the node movement is matched with the solution, is the crucial point in the method of dynamic adaptation.

Transformation Function *Q*

In the general case, transformation of the coordinates should be chosen in such a way that in the computational space the derivatives in time should be much smaller than those in the physical space [5, 17, 19]. In addition, the transformation function Q must satisfy the requirement that the solution variation rate should be in a full agreement with the velocity at which the grid nodes move. When the grid nodes move fast enough, their crowding can be unable to keep pace with movement of the solution peculiarities, which can lead to reduction of the adaptation efficiency. If the

grid nodes move too fast, it could lead to either oscillations of the solution or related oscillations of both the grid and the solution.

To compensate incomplete agreement between the sought solution and the mechanism of rearranging the grid, fitting coefficients are usually introduced; by trial and error the coefficients can be chosen so that the inconsistency could be reduced. At the same time, and presence of matching coefficients in the adaptation method is an indication of its imperfection.

To find the required transformation function we shall make use of the quasi-stationarity principle formulated in [17]. The application of this principle makes it possible to find transformation functions that are free from matching parameters. The quasi-stationarity principle is based on the assumption that there exists such a nonstationary system of coordinates in which all the processes proceed in a stationary way, i.e., the solution temporal derivatives are either equal to zero or negligible. For the systems of equations (19)–(20) and (22)–(25) the application of the quasi-stationarity principle amounts to fulfilling the condition

$$\frac{\partial T}{\partial \tau} = \frac{\partial \rho_1}{\partial \tau} = \frac{\partial \rho_2}{\partial \tau} = 0 \tag{26}$$

By solving the systems of equations (19), (20), and (22)–(24), taking into account the condition of (26), with respect to Q_1 and Q_2, the sought transformation functions are obtained:

$$Q_1 = -\frac{\frac{1}{\psi}\left(\mathrm{Le}\frac{\partial}{\partial q}\left|\frac{\partial \rho_1}{\partial q}\right| + \frac{\partial}{\partial q}\left|\frac{\partial T}{\partial q}\right|\right)}{\left|\frac{\partial}{\partial q}(\rho_1 + T)\right| + \mathrm{reg}} - \frac{\left(\frac{\partial}{\partial q}\frac{1}{\psi}\right) * \left(\mathrm{Le}\left|\frac{\partial \rho_1}{\partial q}\right| + \left|\frac{\partial T}{\partial q}\right|\right)}{\left|\frac{\partial}{\partial q}(\rho_1 + T)\right| + \mathrm{reg}} \tag{27}$$

$$Q_2 = -\frac{\left[\mathrm{Le}\left(\frac{\partial}{\partial q}\left|\frac{\partial \rho_1}{\partial q}\right| + \frac{\partial}{\partial q}\left|\frac{\partial \rho_2}{\partial q}\right|\right) + \frac{\partial}{\partial q}\left|\frac{\partial T}{\partial q}\right|\right]}{\psi\left|\frac{\partial}{\partial q}(\rho_1 + \rho_2 + T)\right| + \mathrm{reg}} - \frac{\left(\frac{\partial}{\partial q}\frac{1}{\psi}\right)\left[\mathrm{Le}\left(\left|\frac{\partial \rho_1}{\partial q}\right| + \left|\frac{\partial \rho_2}{\partial q}\right|\right) + \left|\frac{\partial T}{\partial q}\right|\right]}{\left|\frac{\partial}{\partial q}(\rho_1 + \rho_2 + T)\right| + \mathrm{reg}} \tag{28}$$

The first terms in these formulas ensure crowding of the grid nodes. The second terms constrain up to a certain finite value two neighboring nodes from coming close together and serve as a mechanism for automatically controlling the node movement, preventing the node trajectories from intersecting. The factor $\partial/\partial q(1/\psi)$ in the second term, having been substituted in the equation $\partial\psi/\partial\tau = -\partial Q/\partial q$, exerts a repulsing action on the grid nodes. In the case of unconstrained approach of two neighboring [ith and $(i+1)$st] nodes, the corresponding function $\psi_{i+1/2}$ tends to zero. The value of the derivative $\partial/\partial q(1/\psi)$ sharply increases. Accordingly, the repulsing action of the function Q increases sharply as well, preventing the function ψ from vanishing. Recall that the function ψ is the transformation Jacobian and, by the condition of the transformation nondegeneracy, must not become equal to zero. Taking into account a nonmonotonic character of the solution, the first derivatives of the density and temperature in formulas (27) and (28) are taken in moduli. $\mathrm{reg} \ll 1$ is the constant that prevents the denominator from becoming equal to zero at the points where the spatial derivatives vanish. In the computations the value of reg was taken small enough $\mathrm{reg} = 10^{-4}$–10^{-6} that it does not influence the adaptation.

Initial and Boundary Conditions in Variables and Their Modification

In the computational space the initial and boundary conditions (9), (10) take the form:

$$q_0 = 0: \qquad T(q_0,\tau) = \begin{cases} T_0 + c\tau, & \tau \le \frac{1}{c} \\ T_a, & \tau > \frac{1}{c} \end{cases} \qquad J_1(q_0,\tau) = J_2(q_0,\tau) = 0 \tag{29}$$

$$q_L = 1: \qquad J_1(q_L,\tau) = 0 \qquad J_2(q_L,\tau) = 0 \qquad W(q_L,\tau) = 0 \tag{30}$$

$$\tau = 0: \qquad (q,0) = T_0 \qquad \rho_1(q,0) = \rho_0 \qquad \rho_2(q,0) = 0 \tag{31}$$

For inverse transformation equations (21), (25) the boundary conditions are formulated with account of the fact that the functions $Q_{1,2}$ characterize the velocity at which any element moves in the physical space, and since the boundaries of the region under consideration are stationary, the boundary conditions for inverse transformation equations (21), (25) are written in the form:

$$Q_{1,2}(q_0,\tau) = Q_{1,2}(q_L,\tau) = 0 \tag{32}$$

In order to enhance the efficiency of the method of dynamic adaptation, the right-hand boundary condition in (32) is modified in such a way that differential problems (19)–(21) and (22)–(25) should be represented in the form of problems with a free boundary [20, 21]. Assuming that the combustion process is initiated at the left-hand boundary $q = q_0$ and then the combustion wave is propagated across the cold background toward the right-hand boundary $q = q_L$, it stands to reason to exclude the region untouched by perturbation from consideration. For this purpose, at the right-hand boundary the appropriate boundary conditions are formulated, representing the original problem in the form of a problem with a free boundary. To this end, in the interval (q_0, q_L) we choose an arbitrary point $q_f \in (q_0, q_L)$, so that $q_f > q_L$ and $q_f \ll q_L$, and consider it to be a new boundary with the boundary conditions [20, 21]:

$$q = q_f: \qquad T(q_f,\tau) = T_0, \rho_1(q_f,\tau) = \rho_0, \rho_2(q_f,\tau) = 0$$

$$Q_{1,2}(q_f,\tau) = -u = \lim_{q\to q_f} -\frac{\lambda}{C_p T}\frac{1}{\psi}\frac{\partial T}{\partial q} \tag{33}$$

For so long as the perturbation reaches the point $q = q_f$, the boundary remains stationary. Its movement begins with arrival of the heat wave and terminates on reaching the point $q = q_L$. In the final form the boundary and initial conditions for equations (19)–(25) will be written in the form:

$$q_0 = 0: \qquad T(q_0,\tau) = \begin{cases} T_0 + c\tau, & \tau \le \frac{1}{c} \\ T_a, & \tau > \frac{1}{c} \end{cases} \qquad J_1(q_0,\tau) = J_2(q_0,\tau) = Q(q_0,\tau) = 0$$

$$q = q_f: \quad \rho_1(q_f,\tau) = \rho_0, \rho_2(q_f,\tau) = 0, T(q_f,\tau) = T_0, Q(q_f,\tau) = \lim_{q\to q_f} -\frac{\lambda}{C_p T}\frac{1}{\psi}\frac{\partial T}{\partial q} \quad (34)$$

$$\tau = 0: \qquad T(q,0) = T_0 \qquad \rho_1(q,0) = \rho_0 \qquad \rho_2(q,0) = 0 \qquad \psi(q,0) = 1$$

DIFFERENCE SCHEMES AND THEIR NUMERICAL REALIZATION

Difference Approximation of the Differential Model in the Physical Space

To solve numerically the system of equations (19)–(21) and (22)–(25), they are represented in a strictly divergent form. To this end, in the system (19)–(21), Eqs. (19) and (20) are multiplied by the value ψ and then are added to Eq. (21), the latter being multiplied consecutively by ρ and T. The difference approximation of the obtained systems of equations was performed with the help of the conservative finite-difference schemes [22]. In the physical space $\Omega_{x,t}$, a computational grid was introduced with a set of nodes ω numbered by the integer indices (x_i, t^j) and semi-integer indices $(x_{i+1/2}, t^j)$ with the constant step h_x with respect to the spatial variable x and the variable step Δt^j with respect to the variable t:

$$\omega = \left\{ \begin{array}{ll} (x_i,t^j),(x_{i+1/2},t^j), x_{i+1} = x_i + h_x, x_{i+1/2} = x_i + 0.5h & i = 0,1,\ldots,N-1 \\ t^j = t^j + \Delta t^j & j = 0,1,\ldots \end{array} \right\}$$

The flow quantities W_i^j, J_i^j referred to the integer nodes, and the grid functions $T_{i+1/2}^j, \rho_{1,i+1/2}^j, \rho_{2,i+1/2}^j, \Phi_{1,i+1/2}^j, \Phi_{2,i+1/2}^j$ referred to semi-integer points.

For the system of equations (13)–(15), the following family of conservative difference schemes was used:

$$\rho_{1,i+1/2}^{j+1} = \rho_{1,i+1/2}^j - \mathrm{Le}\frac{\Delta t^j}{h_x}(J_{1,i+1} - J_{1,i})^{\sigma_1} - \Delta t^j\left(\beta_1^{-1}\Phi_{1,i+1/2}\right)^{\sigma_1} \quad (35)$$

$$\rho_{2,i+1/2}^{j+1} = \rho_{2,i+1/2}^j - \mathrm{Le}\frac{\Delta t^j}{h_x}\left(J_{2,i+1} - J_{2,i}\right)^{\sigma_2} - \Delta t^j\left(\beta_2^{-1}\Phi_{2,i+1/2} - \beta_1^{-1}\Phi_{1,i+1/2}\right)^{\sigma_2} \quad (36)$$

$$T_{i+1/2}^{j+1} = T_{i+1/2}^j - \frac{\Delta t^j}{h_x}(W_{i+1} - W_i)^{\sigma_3} + \Delta t^j\left(\Phi_{1,i+1/2} + \Phi_{2,i+1/2}\right)^{\sigma_3} \quad (37)$$

$$W_i^j = -\frac{T_{i+1/2}^j - T_{i-1/2}^j}{h_x}, J_k^j = -\frac{\rho_{k,i+1/2}^j - \rho_{k,i-1/2}^j}{h_x}, \Phi_{k,i+1/2}^j$$

$$= \beta_k \rho_{k,i+1/2} A_k \exp\left(-\frac{\theta_k}{T_{i+1/2}^j}\right)$$

where $k = 1, 2$. Differential system (11), (12) was approximated by as similar family, which can be derived if all parameters corresponding to the second reaction are set to zero.

Difference Approximation of the Differential Models in Computational Space

In computational space $\Omega_{q,\tau}$, the computational grid with a set of nodes ω was introduced. The set of nodes was numbered with the help of integer i and semi-integer $i+\frac{1}{2}$ indices. The grid was built with a constant step h with respect to the spatial coordinate q and a variable step Δt^j with respect to the variable τ:

$$\omega = \left\{ \begin{array}{ll} (q_i,\tau^j)(q_{i+1/2},\tau^j), q_{i+1} = q_i + h, q_{i+1/2} = q_i + 0.5h & i = 0,1,\ldots,N-1 \\ \tau^{j+1} = \tau^j + \Delta\tau & j = 0,1,\ldots \end{array} \right\}$$

The flow quantities W_i^j, Q_i^j, J_i^j, and the variable x_i^j refer to the integer grid nodes (x_i,τ^j). The grid functions $T_{i+1/2}^j$, $\rho_{i+1/2}^j$, $\psi_{i+1/2}^j$, $\Phi_{1,i+1/2}^j$ $\Phi_{2,i+1/2}^j$ refer to the semi-integer points $(x_{i+1/2},\tau^j)$.

The divergent form of the system of differential equation (19)–(21) was approximated by the family of conservative difference schemes:

$$(\psi\rho_1)_{i+1/2}^{j+1} = (\psi\rho_1)_{i+1/2}^j - \frac{\Delta\tau^j}{h}\left[\mathrm{Le}(J_{1,j+1} - J_{1,j}) + (Q_1\rho_1)_{i+1} - (Q_1\rho_1)_i\right]^{\sigma_1} - \Delta\tau^j(\psi\Phi_1)_{i+1/2}^{\sigma_1} \tag{38}$$

$$(\psi T)_{i+1/2}^{j+1} = (\psi T)_{i+1/2}^j - \frac{\Delta\tau^j}{h}\left[W_{i+1} - W_i + (Q_1T)_{i+1} - (Q_1T)_i\right]^{\sigma_1} + \Delta\tau^j(\psi\Phi_1)_{i+1/2}^{\sigma_1} \tag{39}$$

$$\psi_{i+1/2}^{j+1} = \psi_{i+1/2}^j - \frac{\Delta\tau^j}{h}\left[Q_{1,i+1} - Q_{1,i}\right]^{\sigma_3} \qquad x_{i+1}^{j+1} = x_i^{j+1} + h\psi_{i+1/2}^{j+1} \tag{40}$$

The finite-difference approximation of the divergent form of the differential model (22)–(25) was made with the help of the conservative difference schemes:

$$(\psi\rho_1)_{i+1/2}^{j+1} = (\psi\rho_1)_{i+1/2}^j - \frac{\Delta\tau^j}{h}\left[\mathrm{Le}(J_{1,j+1} - J_{1,j}) + (Q_1\rho_1)_{i+1} - (Q_1\rho_1)_i\right]^{\sigma_1} - \Delta\tau^j(\beta_1^{-1}\psi\Phi_1)_{i+1/2}^{\sigma_1} \tag{41}$$

$$(\psi\rho_2)_{i+1/2}^{j+1} = (\psi\rho_2)_{i+1/2}^j - \frac{\Delta\tau^j}{h}\left[\mathrm{Le}(J_{2,i+1} - J_{2,i}) + (Q_2\rho_2)_{i+1} - (Q_2\rho_2)_i\right]^{\sigma_2} + \Delta\tau^j\left[\beta_1^{-1}(\psi\Phi_1)_{i+1/2} - \beta_2^{-1}(\psi\Phi_2)_{i+1/2}\right]^{\sigma_2} \tag{42}$$

$$(\psi T)_{i+1/2}^{j+1} = (\psi T)_{i+1/2}^j - \frac{\Delta\tau^j}{h}\left[W_{i+1} - W_i + (Q_2\rho_2)_{i+1} - (Q_2\rho_2)_i\right]^{\sigma_3} + \Delta\tau^j\left[(\psi\Phi_1)_{i+1/2} + (\psi\Phi_2)_{i+1/2}\right]^{\sigma_3} \tag{43}$$

$$\psi_{i+1/2}^{j+1} = \psi_{i+1/2}^{j} - \frac{\Delta\tau^j}{h}[Q_{2i+1} - Q_{2i}]^{\sigma_4}, \quad x_{i+1}^{j+1} = x_i^{j+1} + h\psi_{i+1/2}^{j+1} \tag{44}$$

$$\Phi_{k,i+1/2}^{j} = \beta_k \rho_{k,i+1/2} A_k \exp\left(-\frac{\theta_k}{T_{i+1/2}^{j}}\right), \quad W_i^j = -\frac{T_{i+1/2}^{j} - T_{i-1/2}^{j}}{h},$$

$$J_k^j = -\frac{\rho_{k,i+1/2}^{j} - \rho_{k,i-1/2}^{j}}{h}$$

where $k = 1, 2$, $f_i^{(\sigma)} = \sigma f_i^{j+1} + (1-\sigma) f_i^j$, $1 \le \sigma \le 1$, and σ is the free parameter. By choosing the parameter σ, the degree of implicitness of the difference scheme and the approximation order are controlled. The values of $\sigma_1 = \sigma_2 = \sigma_3 = \sigma_4 = 0$ correspond to the explicit difference scheme of the first approximation order with respect to $\Delta\tau^j$ and the second approximation order with respect to h: $O(\Delta\tau + h^2)$. The choice of the values $\sigma_1 = \sigma_2 = \sigma_3 = \sigma_4 = 1$ corresponds to a completely implicit scheme, with the approximation order being $O(\Delta\tau + h^2)$. In the case of $\sigma_1 = \sigma_2 = \sigma_3 = \sigma_4 = 0.5$, we obtain the only scheme with second order of approximation $O((\Delta\tau)^2 + h^2)$.

For numerical computation the obtained difference schemes (35)–(37) and (38)–(40), (41)–(44) were previously linearized using the Newton iteration method. In transition from the jth temporal layer to the $(j+1)$st layer this method allows representing the sought difference equation in the form:

$$T_i^{j+1} = T_i^j + \delta T_i^{j+1} \qquad \rho_i^{j+1} = \rho_i^j + \delta\rho_i^{j+1} \qquad \psi_i^{j+1} = \psi_i^j + \delta\psi_i^{j+1}$$

By writing difference schemes (35)–(37) and (38)–(40), (41)–(44) with respect to the unknowns $\delta T_i^{j+1}, \delta\rho_i^{j+1}, \delta\psi_i^{j+1}$, we obtain the linear ones at each sth iteration of the system of algebraic equations. From the solutions of these equations the increments of

$$\delta T_i^S, \delta\rho_i^S, \delta\psi_i^S$$

and the values of

$$T_i^{S+1} = T_i^S + \delta T_i^{S+1}, \rho_i^{S+1} = \rho_i^S + \delta\rho_i^{S+1}, \psi_i^{S+1} = \psi_i^S + \delta\psi_i^{S+1}$$

are found. The iteration procedure was terminated when the following condition was satisfied:

$$\left|\delta f_i^{S+1}\right| = \left|f_i^{S+1} - f_i^S\right| \le \varepsilon_1 f_i^S + \varepsilon_2 \qquad \varepsilon_1, \varepsilon_2 \in \left[10^{-3} - 10^{-6}\right]$$

In all computations the integration step $\Delta t^j(\Delta\tau^j)$ was chosen automatically by the number of iterations. Comparison of the computation results obtained using the implicit and symmetrical schemes showed that, with the same accuracy, the symmetrical schemes with $O[(\Delta\tau)^2 + h^2]$ allowed integration with the step being 2–3 times greater.

MODELING OF THE PROCESSES OF ONE-STAGE COMBUSTION

The main purpose of investigation of different combustion modes is to determine the normal propagation velocity u and thermodiffusion structure of the flame front. To analyze numerically the thermoconcentrational structure of the flame front and its propagation modes, we applied two mathematical models formulated in variables of the stationary (x, t) (11)–(12), (13)–(15) and nonstationary (q, τ) (19)–(21), (22)–(25) systems of coordinates, respectively. Combustion models (11)–(12), (13)–(15) in (x, t) variables were used mainly to compare the results and determine the efficiency of the dynamic adaptation method. From the solution of (35)–(37) we determined the spatial-temporal distributions of temperature $T(x, t)$, density $\rho(x, t)$, thickness of the zones of heating $\delta_T(t)$, and diffusion $\delta_{\rho_1}(t)$, as well as the flame front propagation velocity $u(t)$ for one-stage combustion.

At the beginning of each computation the linear law of temperature growth at the left-hand boundary was adopted. As the temperature at this boundary grows, the chemical reaction rate increases sharply. The heat released in the reaction forms the temperature gradient that causes the heat flow directed inside the rod to enhance sharply. As a result, the combustion zone starts moving rapidly toward the right-hand boundary. The character of further propagation of the flame front depends on the values of several decisive parameters. For gaseous media such parameters include the Lewis number Le, characterizing diffusive transport of the gas that has not taken part in the reaction to the reaction zone, and the temperature coefficient of combustion velocity k, characterizing the amount of excessive enthalpy in the front. Combustion of condensed media, which corresponds formally to $\mathrm{Le} = 0$, is characterized by the absence of diffusive flows of the material in the chemical reaction zone, and its structure depends only on the value of the temperature coefficient k.

Depending on the Le–k ratio, there are two qualitatively different modes characterized by either stable or unstable propagation of the flame front.

Stationary Combustion Mode

Stationary combustion modes are realized at values of $\mathrm{Le} \simeq 1$. After the effect of the left-hand boundary condition (the heating wall) has become small, i.e., since the equilibrium between the conductive flow of heat from the reaction zone and heat supply has been set up at the expense of the chemical reaction, the reaction zone starts moving to the right at a constant velocity. The stable combustion mode is set up, for which the typical profiles of the temperature $T(x)$, the density $\rho(x)$, and the function ψ are represented in Figure 1.

The characteristic features of stationary combustion ($\mathrm{Le} = 1$) are a constant front propagation velocity, Figure 2*a*, a similarity of the spatial profiles of temperature $T(x, t)$ and density $\rho(x, t)$, Figures 1*a* and 1*b*, and an approximate equality of the zones of thermal and diffusion effects $\delta_T(t) \approx \delta_\rho(t)$, Figure 2*a*. The temperature maximum is in the front of combustion and coincides with the adiabatic combustion temperature $T_m = T_a(T_a = T_0 + F/c_p)$. Figure 2*a* also represents the temporal dependence of the combustion velocity $u(t)$.

For computation, the main peculiarity of stationary modes of combustion is the presence of a practically permanent spatial zone with sharp gradients

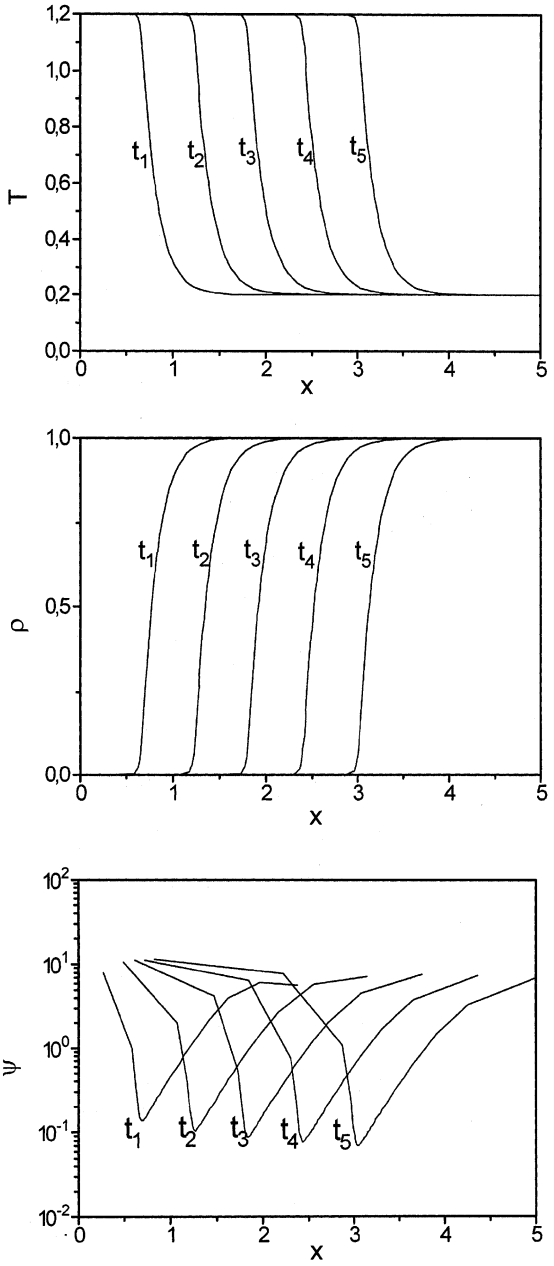

Figure 1. Profiles of temperature, density, and the function ψ at different instants of time for $\mathrm{Le} = 1,\ \theta = 18,\ A = 10^{10},\ N = 40$.

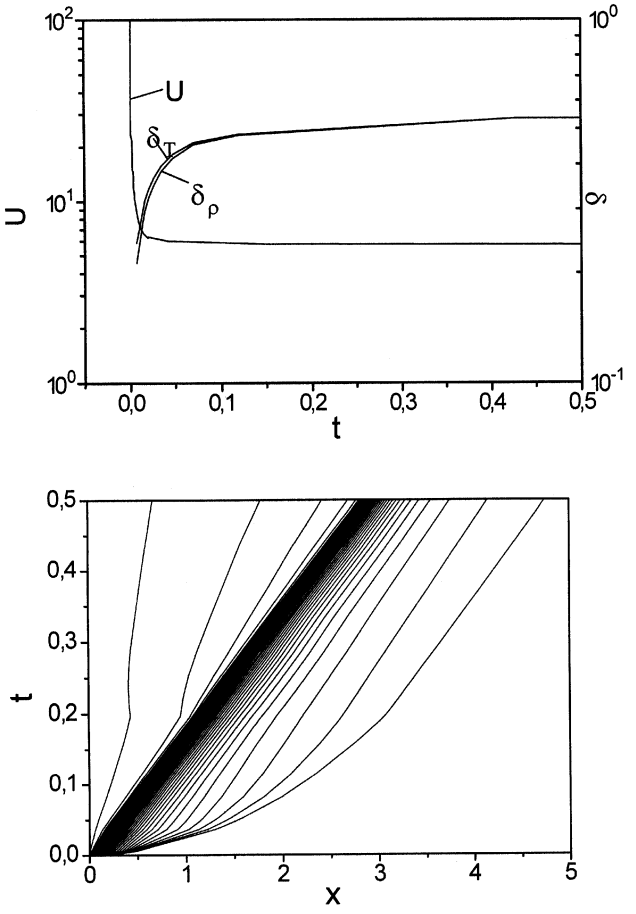

Figure 2. Front velocity U and thicknesses of both the combustion and chemical reaction zones δ_T, δ_ρ and trajectories of moving nodes for Le $= 1$, $\theta = 18$, $A = 10^{10}$, $N = 40$.

$T(x)$ and $\rho(x)$ that is propagated from the left to the right at a constant velocity. The appearance of the zone of strong variations of the solution leads to an automatic rearrangement of the grid nodes, with the nodes concentrating in the combustion zone.

The sharpness of the gradients, in fact, determines the minimal spatial step $h_{x,\min}$. The dynamics of spatial step variation are conveniently characterized with the help of the function $\psi(x) = h_x(t)/h$, Figure 1*c*, which is a dimensionless spatial step in the physical space. The function $\psi(x)$ shows by what factor the grid step with respect to the spatial coordinate $x(t)$ was changes as compared to the initial instant of time $(t = 0, \psi)$. Calculation showed that in the combustion zone the spatial step was reduced by the factor of 10, and in other regions it was enhanced by the factor of 2–5, Figure 1*c*. The trajectories of the moving grid nodes are presented in Figure 2*b*. In the diagram *x(t)*, Figure 2*b*, the combustion front position corresponds to the region of the densest crowding of the trajectories.

Unstable Modes of Combustion

One of the most important factors causing the combustion temperature to change is the instability of the flame front. In laminar modes of combustion the thermodiffusion instability arises in the case of the inequality Le. 1. The more the Lewis number deviates from unity, the greater is the destabilizing action. Transition from one mode to the other occurs at certain critical values of the decisive parameters Le and K [10, 11]. Depending on the Le–K ratio, the thermodiffusion instability may have either a monotonic or oscillatory character.

Monotonic instability. At $\mathrm{Le} \gg 1$ an unstable mode of combustion is realized when the overheated combustible mixture has an excessive enthalpy behind the front and the minimal enthalpy in the front. For example, at $\mathrm{Le} = 10$ and a sufficiently high value of the temperature coefficient of velocity K (the value of K is controlled by choosing value of the activation energy θ), the combustion mode is realized in which the zone of diffusion action turns out to be significantly larger than that of heating $\delta_{\rho_1}(t) > \delta_T(t)$. Since the diffusion processes prevail, the chemical energy carrier is being carried away from the combustion zone and the total enthalpy in the front turns out to be minimal. The combustion temperature behind the front turns out to be higher than the adiabatic temperature, $T_{\max} > T_a$, Figure 3*a*. The maximal overheating is achieved at the initial instants of time, Figure 3*a*, and then the process proceeds at a gradually decreasing rate. The instability attains a monotonic character, which is in good agreement with the linear theory [8, 11].

As for calculation, the combustion modes with $\mathrm{Le} \gg 1$ differ little from the mode with $\mathrm{Le} = 1$. As in the previous case, the adapting grid nodes get concentrated in the front region of the greatest steepness. At $\mathrm{Le} \gg 1$ the temperature profiles $T(x)$, Figure 3*b*, have the greatest steepness.

Oscillatory instability. The character of instability varies qualitatively in the case of inverse relation of the transfer coefficients $D \ll a$, which corresponds to the values $0\ \mathrm{Le} < 1$. As the Lewis number decreases, the diffusion flow toward the combustion zone also decreases and the thermal action zone becomes larger, $\delta_T(t) > \delta_{\rho_1}(t)$. When the condition $K > K_c$ is fulfilled, the role of destabilizing factors is enhanced. In the case of combustion without gas ($\mathrm{Le} = 0$), the instability is determined entirely by the temperature coefficient of the combustion velocity K [9]:

$$K = (T_a - T_0)\frac{d\ \ln u}{dT_0} > K_c$$

An explicit expression of the temperature coefficient depends on the kind of the stationary law of combustion $u(T)$. In the case of the Arrhenius dependence of the chemical reaction velocity (1) $u \sim \exp(-E/2RT_a)$, the instability condition assumes the form:

$$K = \frac{(T_a - T_0)}{2RT_a^2}E < K_c, \quad K_c = 4.24$$

[9, 10]. As the Lewis number becomes greater ($0 < \mathrm{Le} < 1$), the value of K_c increases [10].

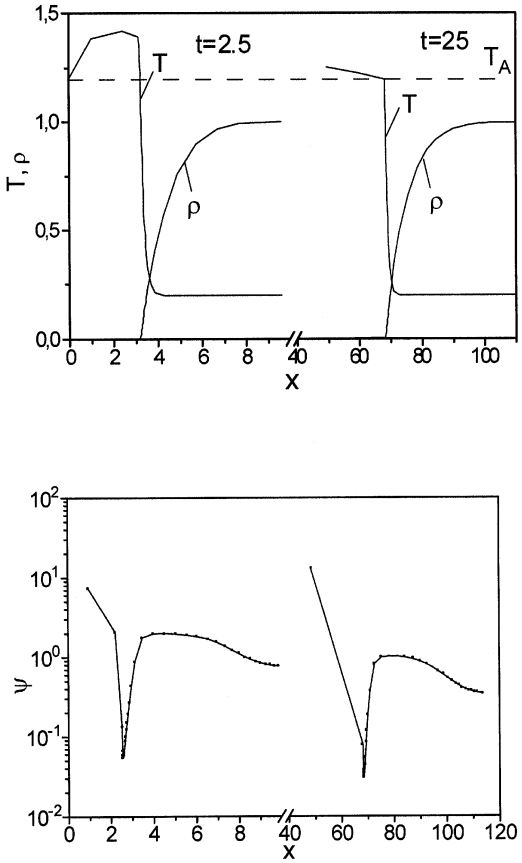

Figure 3. Profiles of temperature, density, and function ψ for Le = 10, $\theta = 18$, $A = 10^{10}$, $N = 40$.

At first, instability of combustion is manifested in the forms of attenuating oscillations. Farther and farther from the stability threshold, which is due to a sharp decrease of the Lewis number $\mathrm{Le} \ll 1$ or a significant growth of the coefficient K, the discrepancy between the characteristic scales $\delta_{\rho_1}(t)$ and $\delta_T(t)$ becomes much greater, which gives rise to a considerable enthalpy excess in the front. A heat excess in the combustion front results in the instability acquiring a marked oscillatory character. The amplitude, the frequency, and the structure of oscillations vary with distance from the stability threshold. At a fixed value of θ and with an increasing Lewis number, the amplitude and the frequency of oscillations are increased and the oscillation structure assumes a form close to that of harmonic oscillation. Beginning from certain values of Le and K, the oscillations no longer depend on the heating wall and a self-oscillation mode of combustion is realized in the system (Figures 4 and 5).

Propagation of the combustion front in the oscillatory mode is a sequence of periodically alternating stages of bursts and depressions, which correspond to maximums and minimums of the temperature and velocity, respectively (Figures 4 and 5).

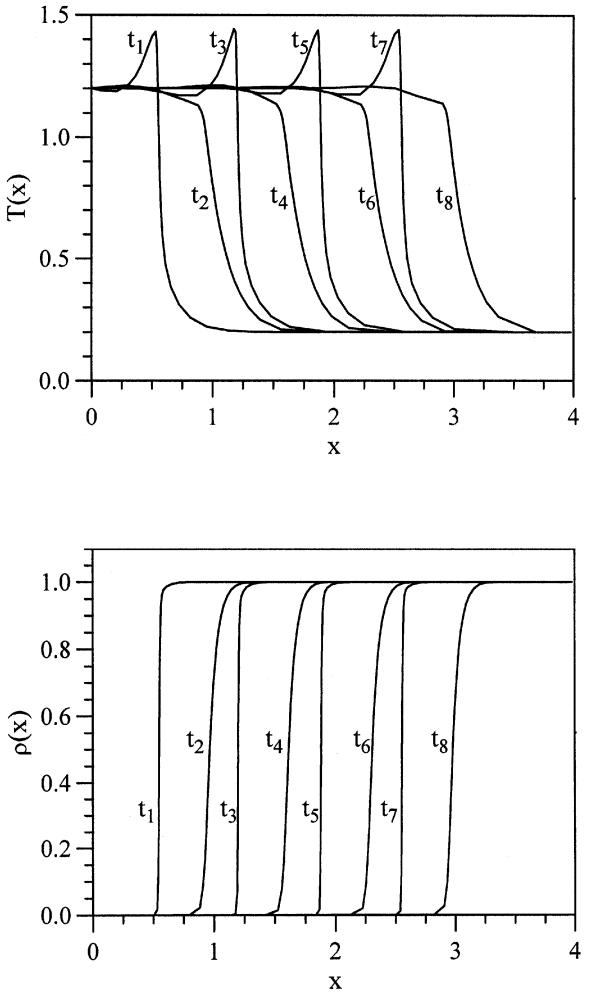

Figure 4. Spatial distribution $T(x)$ and $\rho(x)$ at different instants of time $t_1 - t_8$ for Le $= 0.3$, $A = 10^{10}$, $\theta = 18$, $N = 33$.

The time instants with odd indices correspond to positions of bursts; those with even indices, depressions. At an instant of burst the temperature behind the front exceeds that of stationary adiabatic combustion. In the diagram of moving nodes these oscillations correspond to periodic crowding of the grid nodes (Figure 5*b*).

At the times of bursts, which correspond to maximal values of temperature and velocity, the grid nodes are concentrated in the zones of thermal and diffusion fronts, which is shown in the dependencies $\psi(x)$ in the form of abrupt troughs. The temperature maximum in Figure 4*a* corresponds to the combustion velocity maximum in Figure 6*a* and the minimal values of $\delta_{\rho_1}(t)$ and $\delta_T(t)$. A high velocity assists fast burning of the heated layer. As the dimensions of the heated layer are reduced, the spatial gradients T and ρ becomes steep, Figures 4*a* and 4*b* which encourages an intense thermal transfer from the reaction zone and the onset of the depression stage.

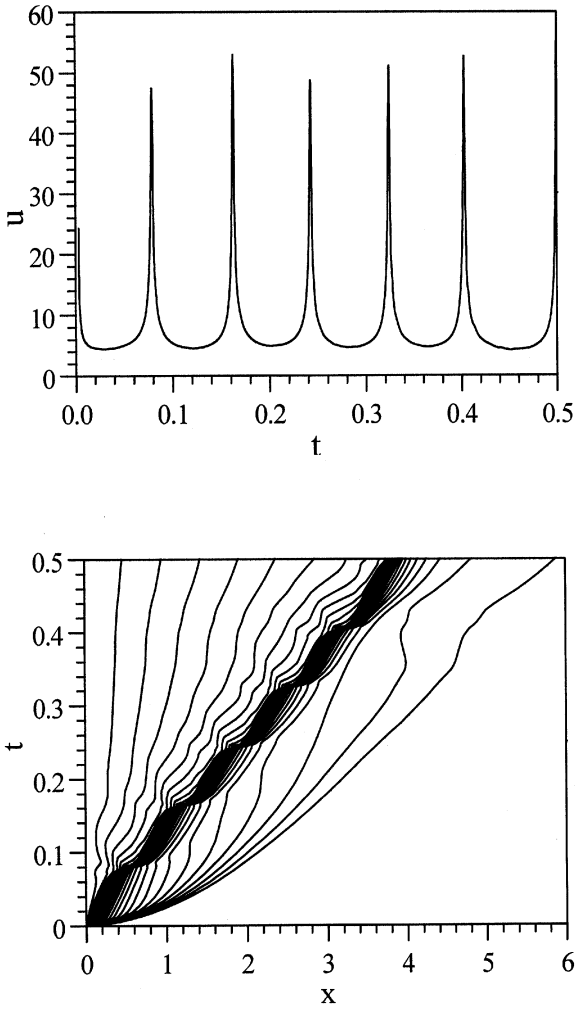

Figure 5. Combustion front velocity and diagram of moving nodes for Le = 0.3, $A = 10^{10}$, $\theta = 18$, $N = 33$.

At the depression stage the heated zone is recovered at the expense of the thermal flow from the zone of the burnt material and, as a consequence, the temperature (and accordingly, the velocity) behind the combustion front is lowered. By the end of the depression stage a thick layer of the heated agent is formed, which bursts again.

Pulse dynamics. Calculations showed that self-oscillation combustion modes are realized within a narrow range of Le and K values. Farther and farther from the self-oscillation threshold, as the Lewis number decreases or θ_1 increases, the pulse structure is changed, At a fixed θ_1, a decrease in Le results in growth of the amplitude and frequency of oscillations. An increase in θ_1, with a fixed Le, leads to growth of the amplitude and period of oscillations. In both cases the burst duration is reduced and depression duration is increased. The oscillation period can be estimated as proportional to $\mathrm{Le} \cdot A_1^{-1} \exp(\theta_1)$.

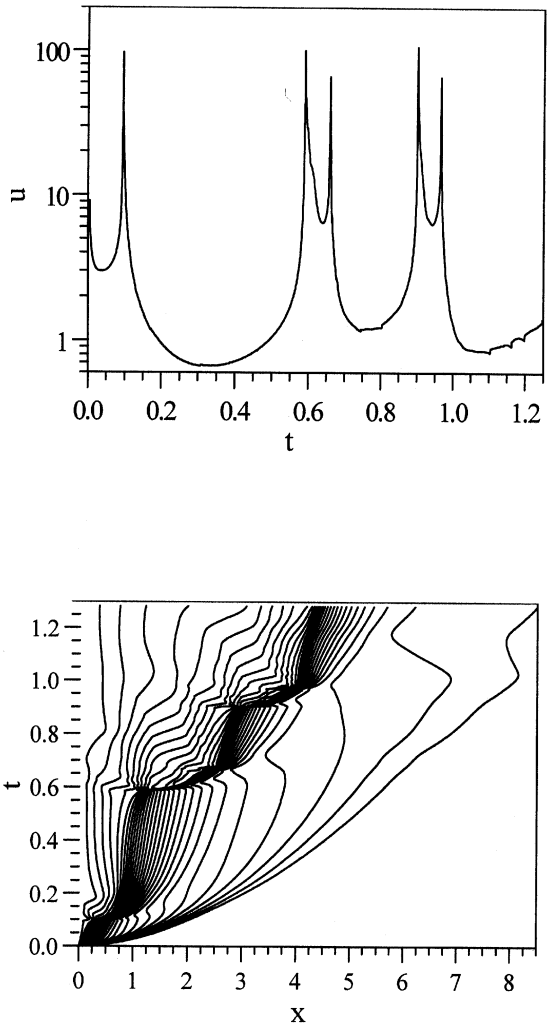

Figure 6. Combustion front velocity and diagram of moving nodes for $\mathrm{Le} = 0.1, \mathrm{A} = 10^{10}, \theta = 18, N = 33$.

A further decrease in Le and an increase in K result in destruction of self-oscillations. The amplitude and frequency of pulses are growing, and the oscillations attain a more expressed relaxation character, when the depression stage duration is still further increased and the burst duration is reduced, Figure 6*a*. A decrease in the Lewis number to values of $\mathrm{Le} \approx 0.1$ results in pulses of a complex structure, when several velocity peaks are observed within one period, Figure 5*a*. A complex character of the solution predetermines a complex mechanism of grid rearrangement when the minimal spatial step is decreased by about three orders. The complexity of this rearrangement can be seen in the diagram of the moving nodes represented in Figure 6*b*, which corresponds to the total number of nodes $N = 33$.

The greatest difference between the zones of thermal and diffusion actions was observed in combustion of condensed media for which $\mathrm{Le} = 0$. In this case the

thickness of $\delta_{\rho_1}(t)$ can be identified with the spatial dimensions of the chemical reaction zone, whose characteristic dimensions are much smaller that those of the heated layer. The diffusion of the combustible mixture components is an additional stabilizing factor, and the absence of the diffusion in the combustion zone of condensed medium is responsible for the minimal resource of stability of their combustion.

In conclusion, it should be noted that layer-by-layer pulsing modes of propagation of the reaction front were mainly observed experimentally in condensed media [23].

MODELING OF PROCESSES OF TWO-STAGE COMBUSTION

Introducing the second chemical reaction into consideration complicates the general course of the process, which in this case is described by relations of thermophysical and kinetic parameters of both reactions. Let us consider the effect of the second reaction on the flame front stability.

Stable Modes

The appearance of the second reaction is manifested in the first place in variation of the flame front structure. The heat content in the front is determined by the relation of the spatial scales of the three zones: the thermal zone δ_T and two diffusion zones δ_{ρ_1} and δ_{ρ_1}. As shown by calculations, the stable modes of the flame front propagation can be realized under the conditions when the thickness of one diffusion zone is greater and that of the second diffusion zone is smaller than the size of the thermal zone. As in the one-stage variant, stable modes are realized at $\mathrm{Le} \simeq 1$.

Figures 9*a* and 9*b* represent characteristic distributions of density $\rho_1(x), \rho_2(x)$, temperature $T(x)$, and the function ψ for two instants of time. One can see that the interaction of the zones of thermal and diffusion actions has a complicated nature, however, in the course of time a stable relation $\delta_{\rho_1}(t) < \delta_T(t) < \delta_{\rho_2}(t)$, is set up, which corresponds to a constant value of the velocity $u(t)$.

In general, the influence of the second reaction in the stationary case $\mathrm{Le} \simeq 1$ is manifested in slowing down the combustion process and decreasing the flame front propagation velocity. The zone of stable combustion by the Lewis number becomes much wider than that in the one-stage variant. The oscillation threshold for two chemical reactions is shifted toward smaller values of Le. Calculations showed that, at fixed values of the parameters for the first reaction in the two-stage case, it may be that the oscillations do not arise, although they were present in the one-stage case.

The distributions of the function ψ and the trajectories of moving nodes $x(t)$ represented in Figures 7*b* and 8*b* indicates that the majority of the grid nodes are concentrated in the combustion zone in proportion to the solution gradients.

Unstable Modes

The reasons and conditions for appearance of oscillation instability at $\mathrm{Le} < 1$ in the two-stage combustion do not differ qualitatively from those of the one-stage process. The main reason for oscillations to appear is the presence of excessive

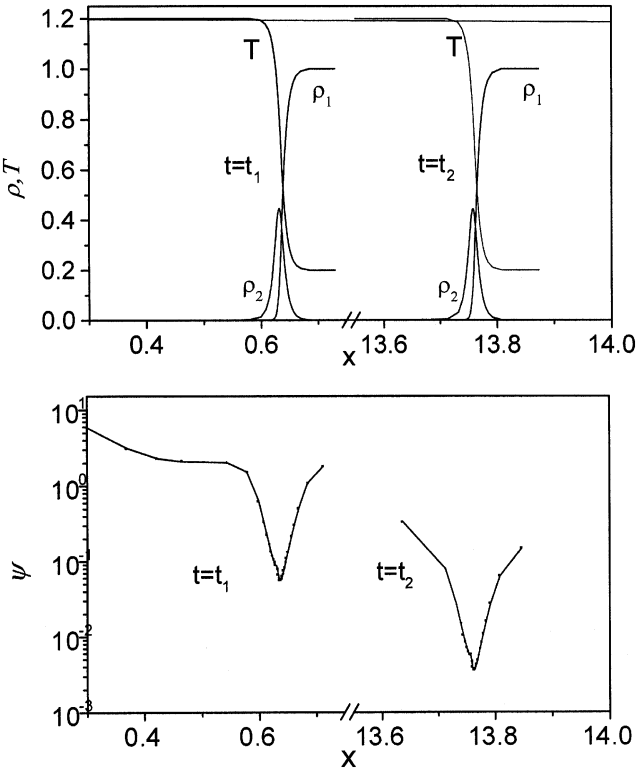

Figure 7. Spatial profiles of temperature T, densities ρ_1, ρ_2, and function ψ at two instants of time, $t_1 = 5 \times 10^{-3}$ and $t_2 = 13$ for Le $= 1$, $\theta_1 = \theta_2 = 4$, $A_1 = 10^7$, $A_2 = 10^6$, $N = 40$.

enthalpy in the front, which arises when the relations $\delta_T(t) > \delta_{\rho 1}(t)$ and $\delta_{\rho 2}(t)$ are executed. Monotonic instability appears when the size of the diffusion action zone significantly exceeds the size of the heating zone $\delta_{\rho_1}(t), \delta_{\rho_2}(t) \ll \delta_T(t)$.

The pulse structure in the two-stage combustion becomes even more complex. In the case of the one-stage pulsing mode there were double bursts, whereas in the two-stage variant four velocity peaks are observed within one period, Figures 8*a* and 8*b*. A similar complex evolution occurs in the combustion zone, Figure 8*c*, where, in the mode of oscillation instability, the relation $\delta_T(t) > \delta_{\rho_1}(t), \delta_{\rho_2}(t)$ must be fulfilled. In this case the spatial distribution of temperature may contain two local maximums: in the front and at the trailing edge of ρ_2. The amplitude, frequency, and structure of pulses depend strongly on the values of the kinetic coefficients of the second reaction, A_2 and ρ_2. Thus an increase in the parameter θ_2 by unity leads to a sharp increase in the number of bursts during the period 8–9. As for computation, the introduction of the second chemical reaction in unstable modes does not lead to any serious complications, although the number of the grid nodes $N \approx 80$ is increased. Figure 9*b* represents the node trajectories corresponding to the case of a strong instability, while Figure 9*a* shows trajectories for the stable case. In the instable regime the grid nodes are crowded in the combustion zone where there are two regions of strong variation in the solution. The former is determined by the position of the fronts

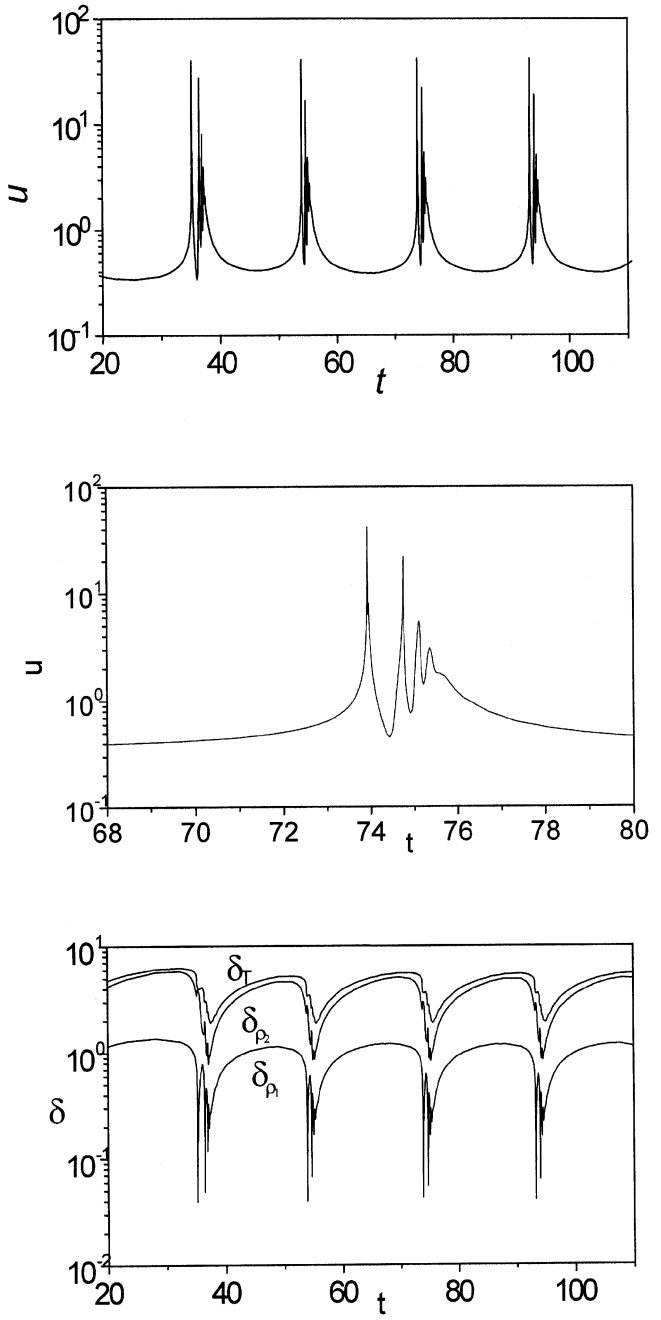

Figure 8. Profile of velocity with its increased fragment and structure of the combustion zones $\delta\rho_1\delta\rho_2$, and δT at $\mathrm{Le} = 0.1, \theta_1 = 17, \theta_2 = 23, A_1 = 2 \times 10^{10}, A_2 = 2 \times 10^9$, $N = 80$.

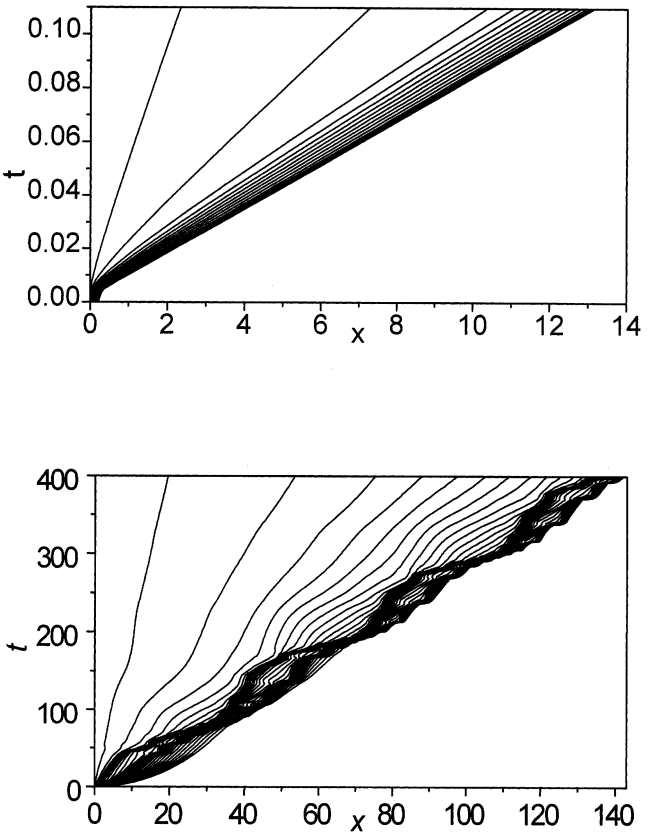

Figure 9. Trajectories of moving nodes at Le $= 1, \theta_1 = \theta_2 = 4, A_1 = 10^7, A_2 = 10^6, N = 40$ and Le $= 0.1$, $\theta_1 = 17, \theta_2 = 24, A_1 = 2 \times 10^{10}, A_2 = 2 \times 10^9, N = 80$.

T, ρ_1, and ρ_2, which are almost coinciding. The latter is determined the trailing edge of the density ρ_2.

EFFICIENCY OF THE DYNAMIC ADAPTATION METHOD

The principal advantage of adapting grids is the possibility of making calculations using a small number of nodes. As an example of mathematical modeling of stationary and nonstationary modes of one-stage combustion, we obtained a quantitative evaluation of the efficiency of the method of dynamic adaptation. In quantitative terms, the efficiency of this method was characterized by two factors: the operation speed t_e and the number of the nodes used n_e. The factors t_e and n_e were determined by comparing the processor time expenditure $t_e = t_f/t_a$ and the number of the nodes used $n_e = N_f/N_a$ in the algorithms using dynamic adaptation t_a, N_a and the algorithms using the grids with fixed numbers of nodes t_f, N_f. The dependence of t_e and n_e on the ratio of the flame front thickness δ to the size of the computation region $L, \delta/L$, was considered as a measure of efficiency. The thickness and velocity

of the flame front were easy to vary by varying the values of Le and $\alpha(\theta)$. It is evident that as the value of δ/L decreases, the expenditure of computation time and the number of nodes increase.

Calculations showed that the minimal number of nodes necessary for solving typical problems of combustion using adapting mashes is ~20–30. All subsequent calculations using adapting nodes were performed with the same number of nodes, $N = 40$. This number was sufficient to make calculations within a wide range of varying parameters Le, θ, and A. The calculation region size L was taken to equal 10; the number of nodes in the grids with fixed nodes was chosen so that the maximum error in velocity was no greater than 1%. In stationary modes of combustion the required accuracy was determined by converging values of the flame propagation velocity on the consistently crowding grids.

To determine the efficiency of adapting grids under conditions of stationary combustion, a series of calculations was performed for fixed values of $A = 10^8$ and Le = 1 and activation energy θ varying in the range 4–17. The results of calculations were compared with similar results obtained using the grid with fixed nodes. For the modes with Le = 1, Figure 10 represents the dependence of the operation speed factor t_e on the ratio δ/L. When θ varies from 17 to 4, the thickness of the chemical reaction zone is two orders of magnitude smaller. Accordingly, the ratio of the size of the reaction zone to the region size $\delta_{\min}/L$ decreases from 0.2 to 2×10^{-3}. The ratio of the processor time expenditure, $t_e = t_f/t_a$, increases from 0.8 to 18. In all the calculations the number of nodes of the adapting grid was constant, $N_a = 40$, and for the fixed-node grid the number of nodes increased from $N_f = 500$ to $N_f = 6,000$. Thus, in computations of stationary combustion modes the efficiency factor $n_e = N_f/N_a$ of the dynamic adaptation algorithms lies in the range of 10–150 with respect to the number of nodes used. The maximum operation speed efficiency for the dynamic

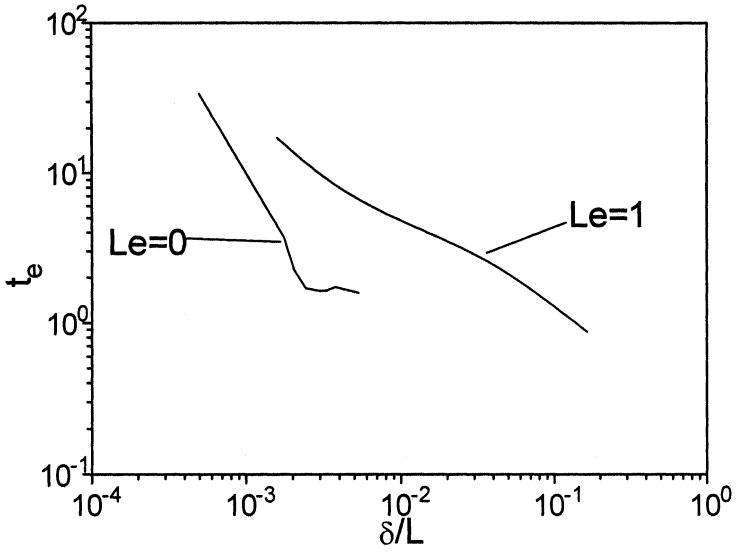

Figure 10. Operation speed efficiency of dynamically adapting algorithms at Le = 1 and Le = 0.

adaptation algorithms is as high as t_e 20. However, if the dimensions of the combustion zone are comparable with those of the region under examination, the operation speed efficiency of the dynamic adaptation grids is noticeably reduced. When the relation $\delta/L \approx 0.2$, the algorithm with the fixed grid is faster by about 20%.

The efficiency of the dynamic adaptation method as applied to the nonstationary combustion mode was investigated at Le = 0. In Figure 10 the dashed curve represents the dependence $t_e(\delta_{\min}/L)$ characterizing the operation speed efficiency of the dynamic adaptation for Le = 0. The region of $\delta/L \approx 2 \times 10^{-3}$ corresponds in the plot to the transition from the stationary combustion mode ($\theta \leq 10$) to the oscillation mode ($\theta > 10$). The operation speed efficiency of the dynamic adaptation method as applied to the oscillating mode of combustion ($\delta/L > 2 \times 10^{-3}, \theta > 0$) is noticeably reduced due to relatively frequent and significant rearrangement of the grid at the instants when bursts or depressions occur. At these instants the reaction zone dimensions vary by tens or hundreds of times. At the transition to the stationary mode ($\delta/L < 2 \times 10^{-3}, \theta \leq 10$) the efficiency index $t_e(\delta_{\min}/L)$ rises rapidly, reaching the value 30. In oscillatory modes the high efficiency of adapting grids as for the number of the nodes used becomes particularly noticeable. The value of the index $n_e = N_f/N_a$ in the variants under study is as high as 500.

It should be noted that the given estimations were obtained at fixed dimensions of the calculation region $L = 10$. As the region increases, the operation speed efficiency of the adapting grid becomes even higher. Its growth is proportional to about $L^{(0.4-0.5)}$.

CONCLUSION

A method of dynamic adaptation is proposed in which the calculation grid is constructed on the differential level. The method is based on the idea of transition to an arbitrary nonstationary system of coordinates. The transformation of the coordinated is performed automatically with the help of the sought solution. Finding the solution and constructing the adapting grid are carried out using the numerical solution of the extended differential model.

The required transformation function contains no fitting coefficients and is found from the assumption that the processes are stationary within a new nonstationary coordinate system (the quasi-stationarity principle). The transformation function as found from the quasi-stationarity principle provides complete agreement between evolution of the sought solution and dynamics of the adapting grid nodes, thereby preventing their trajectories from intersecting.

The method allows calculation of nonstationary temperature and concentration fields in problems with mass/energy sources in regions with mobile boundaries.

Examples of calculations of stable and unstable (pulsing) modes of laminar combustion are resented. In all the variants the application of the dynamically adapting algorithms made it possible to raise considerably the efficiency of calculations as compared to that of calculations made using fixed-node grids. Application of the dynamic adaptation allowed the number of nodes to be reduced by 1–2.5 orders and the operation speed to be increased by 2–50 orders of magnitude.

REFERENCES

1. I. Babuska, W. D. Henshaw, J. E. Oliger, J. E. Flaherty, J. E. Hopcroft, and T. Tezduyar (eds.), *Modeling, Mesh Generation, and Adaptive Numerical Methods for Partial Differential Equations*, p. 346, Springer-Verlag, New York, 1995.
2. R. Biswas, J. E. Flaherty, and D. C. Arney, An Adaptive Mesh-Moving and Refinement Procedure for One-Dimensional Conservation Laws, *Appl. Numer. Math.*, vol. 11, pp. 259–282, 1993.
3. S. Achrya and F. H. Moukalled, An Adaptive Grid Solution Procedure for Convection-Diffusion Problems, *J. Comput. Phys.*, vol. 91, pp. 32–54, 1990.
4. W. Huang, Y. Ren, and R. D. Russel, Moving Mesh Methods Based on Moving Mesh Partial Differential Equations, *J. Comput. Phys.*, vol. 113, pp. 279–290, 1994.
5. J. G. Verver, J. G. Blom, and J. M. Sans-Serna, An Adaptive Moving Grid Method for One-Dimensional Systems of Partial Differential Equations, *J. Comput. Phys.*, vol. 82, pp. 454–486, 1989.
6. H. A. Dwyer, Grid Adaption for Problems in Fluid Dynamics, *AIAA J.*, vol. 22, pp. 1705–1712, 1984.
7. V. D. Liseikin, Structured Adaptive Grids Generation Methods Review, *Zhurnal Vychislitelnoy Matematiki i Matematicheskoy Fiziki*, vol. 36, no. 1, pp. 3–41, 1996.
8. J. B. Zeldovich, G. I. Barenblatt, V. B. Librovich, and G. M. Mahviladze, *Mathematical Theory of Combustion and Explosion*, Nauka, Moskva, 1980.
9. K. G. Shkadinskiy, B. I. Haikin, and A. G. Merzhanov, Propagation of Pulsed Front of Exothermic Reaction through Condensed Media, *Fizika Goreniya i Vzryva*, vol. 7, no. 1, pp. 19–28, 1971.
10. G. M. Mahviladze and B. V. Novozhilov, 2-d Instability of Combustion of Condensed Systems, *Zhurnal Prikladnoi Mechaniki i Teoreticheskoy Fiziki*, no. 5, pp. 51–59, 1971.
11. A. M. Grishin, V. N. Bertzsun, and V. M. Agranat, Investigation of Diffusion-Thermal Instability of Laminar Flames, *Dokl. Akad. Nauk SSSR*, vol. 235, no. 3, pp. 550–553, 1977.
12. N. A. Dar'in and V. I. Mazhukin, Mathematical Modeling of Stephan Problem of Adaptive Grid, *Differentzialnye Uravneniya*, vol. 23, no. 7, pp. 1154–1160, 1987.
13. N. A. Dar'in and V. I. Mazhukin, On One Approach to the Adaptive Differential Grids Generation, *Dokl. Akad. Nauk SSSR*, vol. 298, no. 1, pp. 64–68, 1988.
14. P. V. Breslavskii and V. I. Mazhukin, Mathematical Modeling of Pulsed Melting and Evaporation Processes with Explicit Interphase Front Tracking, *Inzhenerno-fizicheskii Zhurnal*, vol. 57, no. 1, pp. 107–114, 1989.
15. V. I. Mazhukin, I. Smurov, C. Dupuy, and D. Jeandel, Simulation of Laser Induced Melting and Evaporation Processes in Superconducting Ceramics. *Numer. Heat Transfer A*, vol. 26, pp. 587–600, 1994.
16. P. V. Breslavskii and V. I. Mazhukin, Dynamic Adaptation in Problems of Gas Dynamics, *Matematicheskoe Modelirovanie*, vol. 7, no. 12, pp. 48–78, 1995.
17. V. I. Mazhukin, A. A. Samarskii, and A. V. Shapranov, Dynamic Adaptation Method in Burgers Problem, *Dokl. Ross. Akad. Nauk*, vol. 333, no. 2, pp. 165–169, 1993.
18. G. R. Otey and H. A. Dwyer, Numerical Study of the Interaction of Fast Chemistry and Diffusion, *AIAA J.*, vol. 17, no. 6, pp. 606–613, 1979.
19. L. Petzold, Observations on an Adaptive Moving Grid Method for One-Dimensional Systems for Partial Differential Equations, *Appl. Numer. Math.*, vol. 3, pp. 347–360, 1987.
20. V. I. Mazhukin and L. Ju. Takoeva, Principles of Adaptive Grid Generation in 1-d Boundary Problems, *Matematicheskoe Modelirovanie*, vol. 2, no. 3, pp. 101–118, 1990.

21. V. F. Vasilevskii and V. I. Mazhukin, Numerical Computation of Temperature Waves with Contact Discontinuities on Dynamic Adaptating Grids, *Differentzialnye Uravneniya*, vol. 25, no. 7, pp. 1188–1193, 1989. 730
22. A. A. Samarskii, *Difference Schemes Theory*, Nauka, Moskva, 1983.
23. A. G. Merzhanov, A. K. Filonenko, and I. P. Borovinckaya, New Phenomenas in Combusion of Condensed Systems, *Dokl. Akad. Nauk SSSR*, vol. 208, no. 4, 892–894, 1973.